

Journal of Materials Chemistry A

Accepted Manuscript



This is an *Accepted Manuscript*, which has been through the Royal Society of Chemistry peer review process and has been accepted for publication.

Accepted Manuscripts are published online shortly after acceptance, before technical editing, formatting and proof reading. Using this free service, authors can make their results available to the community, in citable form, before we publish the edited article. We will replace this *Accepted Manuscript* with the edited and formatted *Advance Article* as soon as it is available.

You can find more information about *Accepted Manuscripts* in the [Information for Authors](#).

Please note that technical editing may introduce minor changes to the text and/or graphics, which may alter content. The journal's standard [Terms & Conditions](#) and the [Ethical guidelines](#) still apply. In no event shall the Royal Society of Chemistry be held responsible for any errors or omissions in this *Accepted Manuscript* or any consequences arising from the use of any information it contains.

ARTICLE

Three-dimensional conducting oxide hollow nanobead photoanodes: synthesis, characterization, and applications in dye-sensitized solar cells

Cite this: DOI: 10.1039/x0xx00000x

Received 00th January 2014,

Accepted 00th January 2014

DOI: 10.1039/x0xx00000x

www.rsc.org/

Fa-Qian Liu,^{*a} Juan Su,^a Wei Wang,^a Wei-Hua Li,^{*b,c} Hai-Qing Hu,^a Lei Wang,^a and Rong-Xun Li^a

It was reported that liquid-electrolyte-based dye-sensitized solar cells (DSSCs) are “majority carrier” devices where the internal electric field is screened off; accordingly, the electrons travel through the TiO₂ nanoparticles by diffusion rather than drift, resulting “sticky” electrons which undergo frequent trapping and detrapping. We report here the drift transport observed in I⁻/I₃⁻ electrolyte-based DSSCs by using 3-dimensional (3-D) transparent conducting oxide (TCO) such as fluorinated tin oxide (FTO) coated with TiO₂ as photoanodes. By re-allocating the charge transport process, the thin TiO₂ layer (20–30 nm) covering all TCO scaffold leads to a striking reduction in charge transport distance by a factor of 10²–10³. Electrochemical impedance spectroscopy (EIS) study indicates it is viable to establish potential gradient in the 3-D TCO scaffold; thus, the electron transport in this 3-D TCO structure exhibits field-driven drift behaviour, which is verified by the linear dependence of electron lifetime on the photovoltage, along with the virtually independence of electron transport resistance on the bias voltage in spite of the use of liquid I⁻/I₃⁻ electrolyte.

Introduction

Motivated by the potential as a low-cost solar energy conversion technology, DSSCs have been the subject of substantial academic and commercial research over the last two decades.^{1–3} Nevertheless, further increasing the energy conversion efficiency of DSSCs still remains a principle hurdle because electron transport in the TiO₂ layer (normally over 10 μm thick) takes place by field-free random walk⁴ or ambipolar diffusion⁵ as a consequence of strong coupling of electrons and ions at the nanoscopic level. In this regard, transforming the slow diffusive transport process to field-driven drift transport mechanism, a much more efficient process than diffusion for suppressing recombination, should be a potential remedy. Moreover, drift transport also makes it possible to use alternative redox systems with faster reduction kinetics but less overpotential than the traditional I⁻/I₃⁻ system for enhanced photovoltage.^{6–9}

The current state-of-the-art solutions focused on exploring new photovoltaic materials with faster charge transport properties. However, even for the single crystal anatase TiO₂ or ZnO, the conductivity is only a few S/cm.^{10–15} Alternatively, 1-D nanostructured photoanodes exhibit faster collection times due to the directed electron pathways and better crystallinity.¹⁶

¹⁷ Yet, despite the enhanced charge collection efficiency, light-harvesting efficiency deteriorates significantly due to the loss of surface roughness factor (SRF) in 1-D nanowires in comparison with that of a nanoparticle film.¹⁸ In these designs, slow shuttles are desirable to avoid recombination of electrons in semiconductor and the surrounding oxidizing redox species. However, fast shuttles are desirable to reduce the dye⁺ cations promptly. So, it is highly desirable if drift transport behavior can be attained in liquid electrolyte-based DSSCs.

In conventional DSSCs, the TCO is usually a 2-D planar film that allows light penetration, placed at the end of the transport pathways for final charge collection from the photovoltaic layer. This configuration fails to make efficient use of the TCO in terms of its high conductivity and isolation from counter charges. In contrast, the electron drift mobility in TCO (65 cm² V⁻¹ s⁻¹)^{19, 20} is >10⁷ higher than that in porous TiO₂ (in the range of 10⁻⁷–10⁻⁶ cm² V⁻¹ s⁻¹).²¹ To optimize the charge transport logistics, we propose to transform the conventional planar 2-D TCO electrodes to 3-D TCO nanoarchitected electrodes.^{22–24}

The morphology of TCO is perhaps the most overlooked part in past photovoltaic research, since planar FTO and ITO glass substrates are readily available from commercial sources, which tends to discourage innovation in this critical component. Here,

we report the fabrication of a 3-D nanostructured FTO electrode by using polystyrene (PS) beads as template. The process is illustrated in Fig. 1. Then, a conformal layer of TiO₂ with a thickness of 20~30 nm is deposited on all the inner and outer surfaces of the 3-D FTO hollow nanobead electrodes. The use of 3-D TCO will drastically enlarge the interface area between the FTO and the PV layer such as TiO₂ where light-induced charge separation reactions occur. When the thickness of the TiO₂ layer is thinned to be comparable to the width of the space charge layer at the FTO/TiO₂ semiconductor interface, the build-in potential at FTO/TiO₂ interface will provide a favorable Fermi-level gradient to separate electron-hole pairs and sweep electrons from TiO₂ into FTO,²⁵⁻²⁸ leaving the majority of the transport in the nearly metallic 3-D FTO scaffold for enhanced photocurrent collection. As a result, the slow diffusive transport process can potentially be transformed to a field-driven drift transport mechanism, a much more efficient process than diffusion for suppressing recombination.^{6, 29-31} Upon dye-sensitization, the TiO₂-coated 3-D FTO architecture is used as photoanodes in further DSSC studies.

Experimental

The 3-D FTO hollow nanobead electrodes were prepared by a template-assisted and morphology-controllable evaporative co-assembly method reported in our previous work.²⁴ To suppress the back electron transport, a compact TiO₂ layer was coated by immersing the 3-D FTO nanobead electrode into a 0.2 M TiCl₄ aqueous solution at 80 °C for 40 min. After TiCl₄ hydrolyzed, the electrode was washed with DI water to remove the residual TiCl₄, and then the TiCl₄ treated electrode was sintered at 500 °C in air for 30 min. After coating, electrodes were immediately soaked in an ethanolic solution of 0.5 mM (Bu₄N)₂ [Ru(4,40-dicarboxy-2,20-bipyridine)₂-(NCS)₂] (N719) overnight. The samples were then rinsed with ethanol and dried with a N₂ stream.

The dye-sensitized solar cells were sealed together by sandwiching dye sensitized TiO₂ coated 3-D FTO nanobead photoanode with the Pt-coated FTO cathode using a piece of hot melt surllyn (25 μm thick, Solaronix) as spacer and EL-HSE (Dyesol) as electrolyte. The holes

were sealed using a small piece of hot-melt polymer and a microscope cover slip. The typical active photoelectrode area was 0.36 cm². Traditional TiO₂ (Degussa P25) nanoparticle-based DSSCs with thickness of 8 μm were also prepared for comparison as needed.

The J-V curves and electrochemical impedance spectroscopy (EIS) measurements of the DSSCs were measured on an electrochemical workstation (CHI660D, Shanghai Chenhua Device Company, China) with a simulated solar light with intensity of 100 mW cm⁻² from a xenon arc lamp (XQ-500W, Shanghai Photoelectricity Device Company, China) in ambient atmosphere. Transmission line model was used to fit the impedance data with the help of Z-view 2.9c (Scribner Associates). The dye loading was measured by completely desorbing the sensitized photoelectrodes in 10 mM KOH solution for 2 hours. The absorbance of the resulting pink solutions and three calibration solutions were measured. According to Beer's law, the concentration of the target solution can be obtained by fitting the absorbance at 522 nm (with respect to blank solvent) to the calibration curve.

Results and Discussion

As illustrated in Fig. 1, The monodispersed FTO hollow nanobeads were prepared by a facile one-pot procedure using sulfonated PS beads suspension (526 nm) mixed with FTO precursors (SnCl₂ · 2H₂O and NH₄F) at room temperature to form a precursory gel which can fully surround the surface of the PS templates.^{24, 32, 33} After drying and calcination, solid 3-D FTO hollow nanobead film was formed. Then, all the inner and outer surfaces of the 3-D FTO scaffold along with the continuous underneath FTO substrate are coated with a conformal layer of rutile TiO₂ (20-30 nm). Upon dye-sensitization, both the inner and outer TiO₂ layers serve as light harvesting and charge separation layers, and suppress the electron back transfer from FTO (both 3-D FTO scaffold and the planar FTO substrate) to electrolyte and/or to dye⁺ cations (shunt leakage)^{34, 35} Finally, the 3-D structure is used as photoanodes in further DSSCs studies.

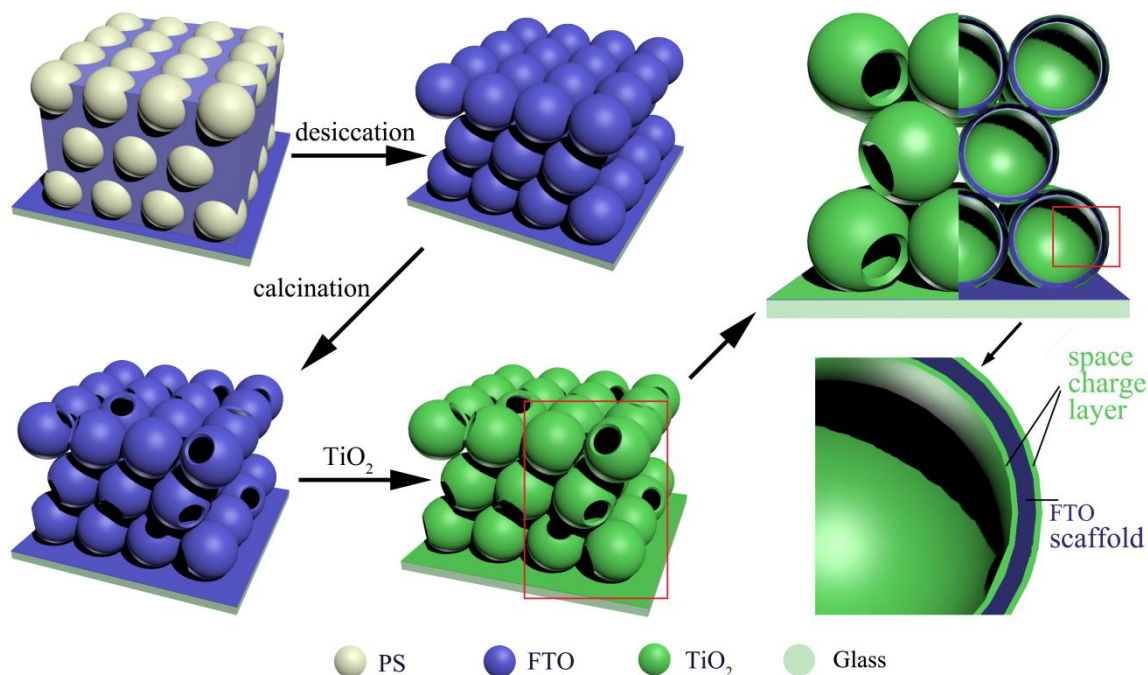


Fig. 1 Schematic design for fabricating TiO_2 -coated 3-D FTO photoanode architecture.

Fig. 2a shows the top SEM image of the FTO hollow nanobeads with apertures of ~ 100 nm resulting from the release of gaseous species from the decomposed templating polystyrene nanobeads which were calcinated at 450°C . These openings ensure the efficient use of the inner and outer surfaces of the hollow nanobeads, while offering passages for the electrolytes to pass through. We can see from the TEM image (Fig. 2b) that these monodispersed hollow spheres have a wall thickness of ~ 60 nm. The TEM image also confirms that the inner cavity diameter is ~ 480 nm. As shown in the cross-sectional SEM image (Fig. 2c), the hollow sphere morphology is omnipresent in the 3-D FTO film. Our previous study showed that the sheet resistance of the 3-D FTO film on FTO substrates is $\sim 27 \Omega/\text{square}$, which indicates the conductivity of our nanobead electrode is excellent comparing to the $\text{M } \Omega/\text{square}$ level of TiO_2 nanoparticle electrodes. To suppress the

recombination reactions of the injected electron with the oxidizing agent of the electrolyte (I_3^-), TiO_2 were deposited using TiCl_4 as precursors.³⁶ Fig. 2d shows the TiO_2 layer is conformal and compact with thickness around $20\sim 30$ nm. The successful coating of TiO_2 is further confirmed by the EDX spectrum (Fig. S1). Fig. 2e is the cross-sectional view of the FTO nanobead film, which shows the thickness of the resulting film is $\sim 8 \mu\text{m}$. The TEM diffraction ring (Fig. S2) shows that the as-synthesized 3-D FTO film has a polycrystalline configuration.³⁷ The additional XRD peaks of TiO_2 coated FTO ($2\theta=36.07, 41.25, \text{ and } 54.36^\circ$) (Fig. 2f) verify the existence of rutile phase of TiO_2 . The surface roughness factor (SRF), the ratio of effective surface area/projected substrate area, was calculated to be ~ 89 based on the BET surface area ($21 \text{ m}^2/\text{g}$) and the planar area of the tested samples.²⁴ This is a significant improvement compared to a flat FTO film, whose SRF is 1.

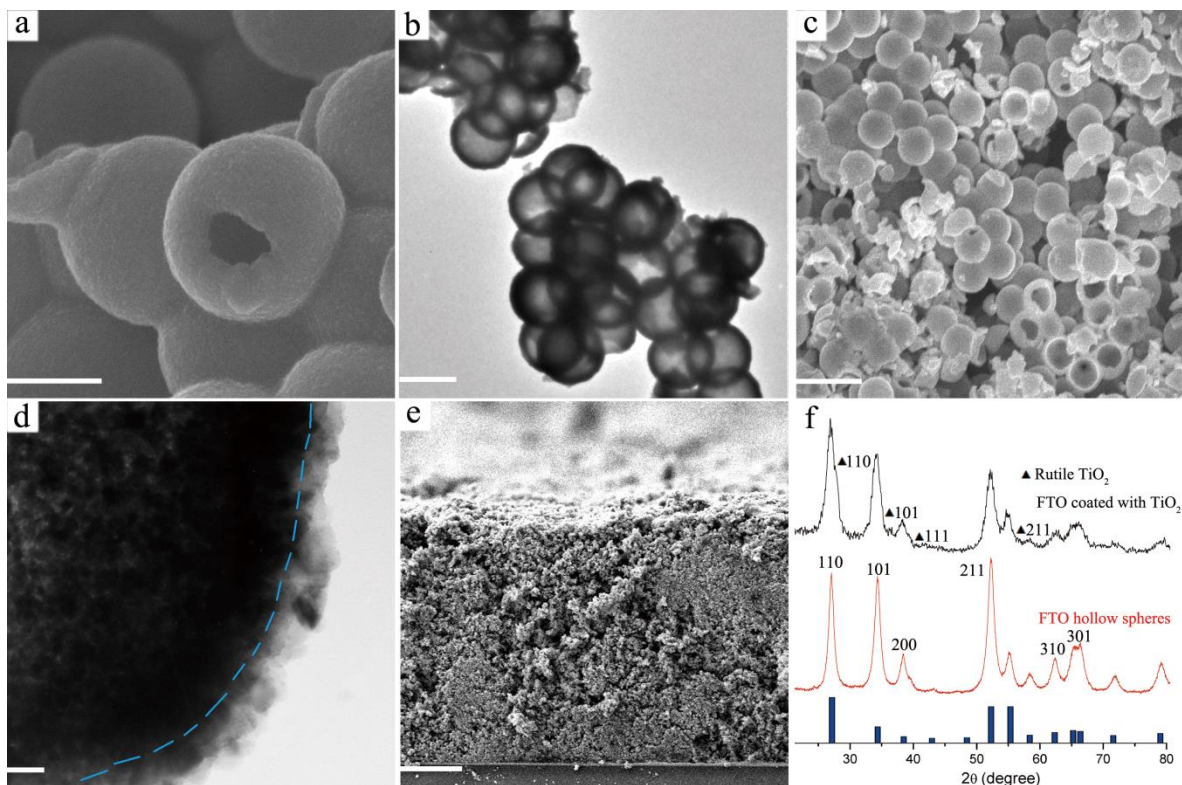


Fig. 2 Morphologies of the 3-D FTO hollow nanobeads. (a) SEM image of monodispersed FTO hollow nanobeads prepared from 526 nm sulfonated PS beads, scale bar: 300 nm. (b) TEM image of the hollow nanobeads of (a), scale bar: 500 nm. (c) The cross-sectional SEM image showing that the hollow nanobeads morphology is omnipresent in the film, scale bar: 1 μm . (d) TEM image of the hollow nanobeads after the coating of TiO_2 , scale bar: 20 nm. (e) The cross-sectional SEM image of the 3-D FTO photoanode, scale bar: 2 μm . (f) XRD spectra of FTO hollow spheres and 3-D FTO coated with TiO_2 .

The photovoltaic parameters of DSSCs based on our TiO_2 coated 3-D FTO film (8 μm thick) with N719 dye as sensitizer and I^-/I_3^- as electrolyte were obtained under one Sun (AM 1.5 G). For a fair comparison, DSSCs based on pure 3-D FTO hollow spheres with a thickness of 8 μm were also measured. Fig. 3 shows the typical J–V curves of the two kinds of DSSCs. The key photovoltaic parameters are summarized in Table 1. The pure 3-D FTO hollow nanobead film is termed as FHNB-P and the 3-D FTO hollow nanobead film coated with TiO_2 is termed as FHNB-T. The measured dye-loading for 8 μm -thick FHNB-T film is around $2.1 \times 10^{-8} \text{ mol/cm}^2$.

Fig. 3 shows the effect of coating one layer of TiO_2 on DSSCs based on 3-D FTO hollow nanobead electrodes. The short-circuit current density (J_{sc}) from the pure 3-D FTO electrode is $\sim 7 \text{ mA/cm}^2$, which is comparable to the values obtained from FTO nanoparticles of the same thickness.³⁵ The open-circuit photovoltage (V_{oc}) of 449 mV, although $\sim 40 \text{ mV}$ higher than that of typical nanoparticle SnO_2 electrodes³⁶ because of Burstein-Moss shift with heavy doping of F,³⁸ is significantly low. After the coating of TiO_2 , the short-circuit current density marginally increases to $\sim 11 \text{ mA/cm}^2$, while the V_{oc} improves remarkably from 449 mV to 749 mV, which is almost comparable to the values obtained from conventional TiO_2 nanoparticles (P25) with the same thickness. The fill factor also increases substantially; here it rises from 33% to 44%, indicating a decrease of the shunt leakage at the

FTO/electrolyte interfaces. Compared to the conventional TiO_2 , we noticed that the fill factor of our cells is still relatively low, primarily because of the unavoidable flawed sites in the TiO_2 shell layer, such as pinholes, which cause the imperfectly sealing of the 3-D FTO scaffold. Atomic layer deposition (ALD), a technique to produce high quality and compact coatings with excellent reproducibility and superior conformal growth on various morphologies, will be used to prevent the shunt leak in the future.

Several factors could contribute to the enhanced photovoltaic parameters. First, LUMO of N719 dye has a less overpotential compared to the conduction band edge of TiO_2 (-4.2 eV vs V_{ac})³⁹ than to FTO (approximately -4.8 eV vs V_{ac}).^{39,40}, resulting in higher V_{oc} of the TiO_2 coated 3-D FTO electrode than pure FTO electrode. Second, the coating of TiO_2 compact layer is believed to effectively reduce the charge recombination at the active layer–electrolyte interface (shunt leak), hence to improve the fill factor and photocurrent density. This is further verified by the smaller dark current found in FHNB-T than that of FHNB-P (Fig. 3). Finally, we assume this improvement can be attributed to the optimized electron transport in our 3-D FTO hollow nanobead photoanode. Under illumination, photoelectrons from excited states of the N719 dyes are injected to the conduction band (CB) of the TiO_2 . Then, the CB edge of TiO_2 inclines to FTO, and the electrons can favorably flow downward from TiO_2 to FTO because of the built-in

potential between TiO_2 and FTO,³⁵ which is further investigated by the electrochemical impedance spectroscopy (EIS).

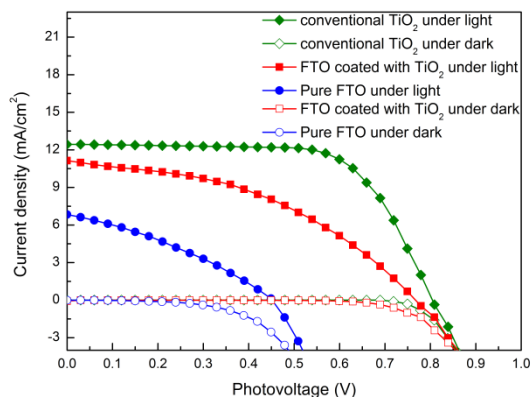


Fig. 3 Typical J-V curves of DSSCs based on pure 3-D FTO, 3-D FTO coated with TiO_2 , and conventional TiO_2 (P25) under an illumination (AM1.5, one Sun) and under dark, respectively. The area of all the devices is 0.36 cm^2 .

Table 1. Photovoltaic Parameters of DSSCs with Same Thickness

Sample	J_{sc} (mA/cm^2)	V_{oc} (V)	FF	η (%)
DSSC based on FHNB-T	11.140	0.749	0.44	3.62
DSSC based on FHNB-P	6.839	0.449	0.33	1.02
$8 \mu\text{m TiO}_2$ (P25)	12.357	0.809	0.67	6.74

We further verified the reduction of the dark current by using EIS technique. Fig. 4a compares the Nyquist plots of FHNB-T-based DSSC with FHNB-P-based DSSC. The EIS data were measured at forward bias of 0.40 and 0.45 V under dark with I^-/I_3^- as electrolyte. The first small arc in the high frequency range of the Nyquist plot (Fig. 4a), which is magnified in Fig. 4b, is assigned to the electron-transfer resistance of Pt and capacitance C_{pt} of the Pt/ electrolyte cathode interface. The low frequency semicircle in Fig. 4a is assigned to the resistance of heterogeneous charge transfer (r_{ct}) from the CB of TiO_2 to triiodide ions in the electrolyte. As shown in Fig. 4a, the increase of diameter of the semicircle from FHNB-P-based DSSC to FHNB-T-based DSSC was observed, indicating that the coating of TiO_2 leads to an obvious suppression of the dark current.

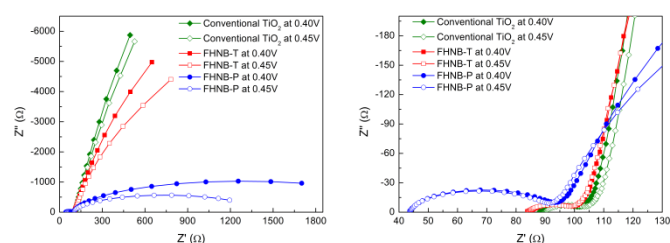


Fig. 4 (a) Nyquist plots of representative EIS data at 400 and 450 mV forward bias under dark for FHNB-T-based DSSC (red square), FHNB-P -based DSSC (blue circle), and conventional TiO_2 (P25)-based DSSC (olive diamond), and (b) their magnified part at high frequency.

Fig. 5 presents the extracted characteristic data by fitting the EIS spectra of the above cells. ZView equivalent circuit modeling software was used to fit the data by utilizing built-in extended element (DX Type 11 – Bisquet #2) which allows for transmission lines modeling (Fig. S3). Fig. 5a shows the resistance of electrons transport (R_{tr}) as a function of forward bias. For conventional TiO_2 film, the transport resistance decreases exponentially with increasing forward bias voltage, which has typically been attributed to the behaviour of “sticky” electrons that undergo frequent trapping and detrapping during their transport and transfer through the mesoscopic TiO_2 network.^{41, 42} However, The R_{tr} values through each FTO/ TiO_2 in our 3-D FTO-based DSSC are independent of the bias voltage, and the measured R_{tr} values at different voltages vary from 5 to 9 Ω , $2-10^4$ times (depending on voltage) lower than those of conventional TiO_2 -based photoanodes, indicating that our 3-D FTO is an excellent transparent material for electron transport, which can be explained by the very thin TiO_2 layer and highly metallic 3-D FTO scaffold. Compared to conventional TiO_2 nanoparticle electrode, the much less dependence of R_{tr} on photovoltage observed in our 3-D FTO-based DSSC suggests that electron transport is favourably dominated by drift mechanism. Thus, the majority transport occurs in the interconnected FTO nanobeads due to the drift of electrons from TiO_2 into FTO driven by the built-in potential at the omnipresent TCO/TiO_2 interface.^{31, 32}

In Fig. 5b, chemical capacitance (C_{μ}) contributed by the electronic states displays a clear exponential dependence with the increase of the applied voltage, both in our 3-D FTO-based DSSC and the conventional TiO_2 -based DSSC. At a given bias voltage, the C_{μ} values of our 3-D FTO-based DSSC are approximately 1~3 orders of magnitude higher than those of conventional TiO_2 -based DSSC. Since C_{μ} is proportional to the electron density and can be expressed as equation 1:

$$C_{\mu} = e^2 n / kT \quad (1)$$

where e is the electron charge, k is the Boltzmann constant and T is the temperature, the increase of C_{μ} shows that electrical communication between the quasi-Fermi levels of TiO_2 and the conducting electron collector (3-D FTO scaffold) is well established, indicating the significant high electron accumulation in the 3-D FTO scaffold. The increase of C_{μ} also reflects the higher density of states (DOS) in FTO ($>10^{21} \text{ cm}^{-3}$, 1~2 orders of magnitude larger than the counter ion, e.g. Li^+)⁴³ than that of TiO_2 . Such high accumulation provides a favorable Fermi-level potential gradient at FTO/ TiO_2 interface (Fig. S4), increases the Helmholtz capacitance at TiO_2 /electrolyte interface,^{25, 28} finally transforming the slow diffusive transport process to a field-driven drift transport mechanism, a much more efficient process than diffusion for suppressing recombination even in I^-/I_3^- -based liquid electrolyte.

Microscopic charge transfer resistance (r_{ct}), which reflects the resistance against the charge recombination events from the phase of high (in TiO_2) to the phase of low Fermi levels (in electrolyte), decreases exponentially with the increase of the applied voltage (Fig. 5c). r_{ct} of 3-D FTO-based DSSC is not as

good as that of the TiO₂-based photoanode because of the imperfect covering of the TiO₂ layer (as thin as 20-30 nm).

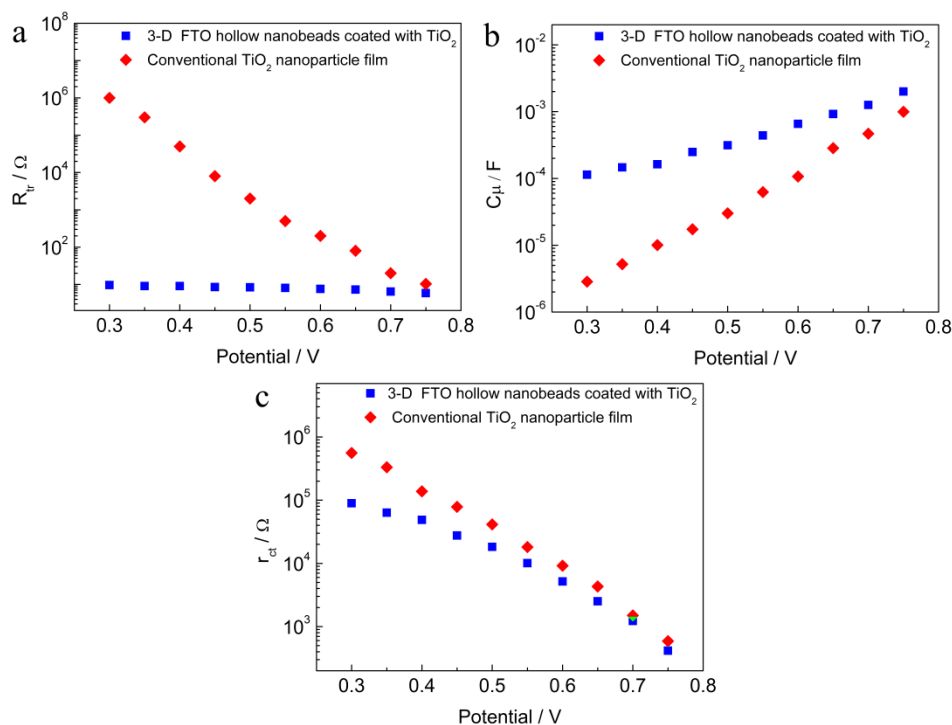


Fig. 5 Fitting results of electron transport resistance R_{tr} (a), chemical potential C_{μ} (b), and interfacial charge transfer resistance r_{ct} (c) for DSSCs based on our 3-D FTO hollow nanobeads coated with TiO₂ (solid square) and conventional TiO₂ (solid diamond) in the dark.

From the fitted data, we could calculate the evolution of parameters such as lifetime $\tau_n = r_{ct}C_{\mu}$ if we assume a classical multiple trapping model.⁴⁴ τ_n shows almost no dependence on the applied voltage for the TiO₂-based cell, which is because the photoelectrons strongly couple with the counterions (e.g. Li⁺ from LiI), which screens off any macroscopic electric fields. Thus, there is no macroscopic drift transport across most of the TiO₂ nanoparticle network. However, in our 3-D FTO-based cell, τ_n decreases linearly with the increase of the applied voltage, showing the existence of an obvious field effect that directs the electron transport in our TiO₂ coated 3-D FTO photoanode. In the case of pure drift transport, where the DOS is overwhelmingly greater than carrier density, such as FTO, a linear relationship is expected for transient photocurrents versus the applied photovoltage, as equation 2:

$$j = en\mu_n \vec{\mathcal{E}} \quad (2)$$

where j is the drift current density, the elementary charge is denoted as e , n and μ_n are the carrier density and effective carrier mobility, while the applied voltage is given by $\vec{\mathcal{E}}$.^{28, 45} Thus, the current (the average drifting speed of electrons) should exhibit linear dependence on applied voltage. Because τ_n in FTO reflects the exposed time of electrons in electrolyte, therefore, it is reasonable to see τ_n exhibit a linear dependence on the bias voltage in drift transport mode as observed in Fig. 6a.

The competition between the collection and the recombination of electrons can be expressed in terms of ratios of the effective

diffusion length to the film thickness (L_n/L), according to $L_n/L = (r_{ct}/R_{tr})^{1/2}$.^{39, 44} As shown in Fig. 6b, the obtained L_n/L increases by about 1 order of magnitude with the bias potential for TiO₂-based DSSC. The calculated electron diffusion length values for 3-D FTO-based DSSC are significantly higher than those of TiO₂-based DSSC, indicating the excellent transport properties. The electron drift mobility in FTO ($65 \text{ cm}^2 \text{ V}^{-1} \text{ s}^{-1}$)^{19, 20} is $>10^7$ higher than that in porous TiO₂ (in the range of $10^{-7} \sim 10^{-6} \text{ cm}^2 \text{ V}^{-1} \text{ s}^{-1}$).²¹ Hence, the electron migration in FTO driven by the Lorentz force can outpace the diffusion of cations in the electrolyte to build up the Hall voltage. Although the cations can eventually counterbalance the Hall voltage through diffusion, but, kinetically, there will be a time lag in cation diffusion due to the much faster electron mobility in FTO than the cation diffusion in electrolyte.

Fig. 6c exhibits the comparison in electron conductivity for both types of devices. The electron conductivity, σ_n , can be derived according to the equation 3:

$$\sigma_n = LBR_{tr}^{-1} \quad (3)$$

where R_{tr} is the macroscopic transport resistance, L is the thickness of the photoanode, and B is the projected area of the photoanode exposed through the Surlyn frame. Compared to the TiO₂-based cell, our 3-D FTO-based photoanode displays greater conductivity at equal applied potentials, which can be attributed to the better conductivity and integrity of the 3-D interconnected FTO scaffold.

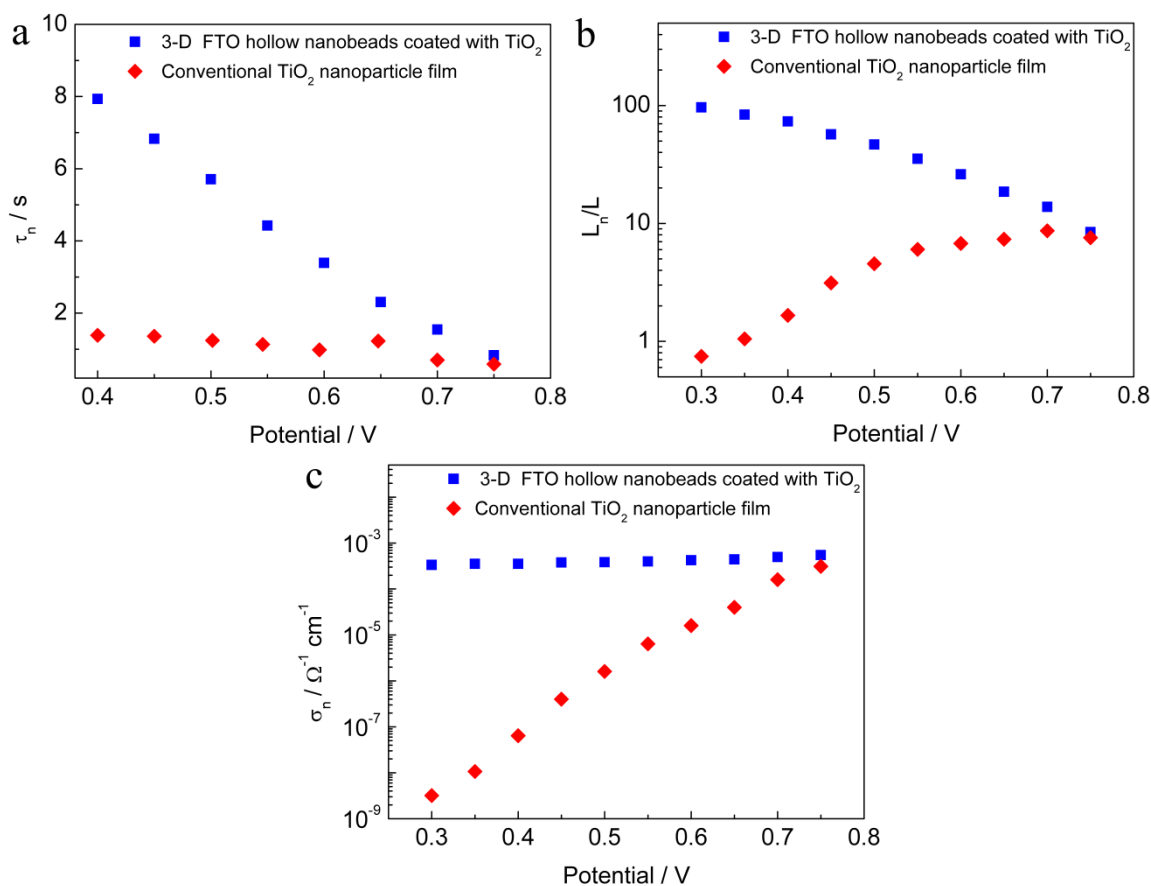


Fig. 6 Derived parameters of electron life time (a), effective diffusion length L_d/L (b), and electron conductivity (c) for DSSCs based on our 3-D FTO hollow nanobeads coated with TiO₂ (solid square) and conventional TiO₂ (solid diamond).

Conclusions

We have successfully synthesized 3-D interconnected FTO nanostructures by morphology-controllable evaporative co-assembly of a colloidal template and prepared TiO₂ coated photoelectrodes. Field-driven drift-transport instead of diffusive transport in liquid electrolyte was observed in our 3-D FTO/TiO₂ photoanode-based DSSCs. EIS suggests that the electron transport resistance is independent on the bias voltage; while the time constants of electron transport exhibit a linear dependence on the bias voltage, a strong indication of drift transport behavior in 3-D FTO hollow nanobeads-based DSSC despite the use of liquid I⁻/I₃⁻ electrolyte. In prospective, this work paves a way for more efficient photovoltaic systems with much faster redox shuttles (relative to I⁻/I₃⁻) with smaller overpotential for a higher attainable photovoltage than the current state-of-the-art.

Acknowledgements

FL acknowledges the support from the National Science Foundation of China (21371105) and the Scientific Development Plan of Qingdao (14-2-4-41-jch). WL acknowledges the support from the National Science

Foundation of China (51179182) and the Distinguished Young Scientists Funds of Shandong (2012JQF01002).

Notes and references

^a Engineering Research Center of High Performance Polymer and Molding Technology, Ministry of Education, Qingdao University of Science and Technology, Qingdao 266042, China. E-mail: faqianliu@yahoo.com.

^b Collaborative Innovation Center of Engineering Construction and Safety for Oceanic Economic Zone, Qingdao 266033, China. E-mail: 1685680@163.com

^c Institute of Oceanology, Chinese Academy of Sciences, Qingdao 266071, China.

† Electronic Supplementary Information (ESI) available: [EDX spectrum, Electron diffraction ring patterns of the 3-D FTO photoanode, and Fermi level (EF) at TiO₂/FTO interface]. See DOI: 10.1039/b000000x/

1. B. C. O'Regan and J. R. Durrant, *Acc. Chem. Res.*, 2009, **42**, 1799-1808.
2. D. Kiessling, R. D. Costa, G. Katsukis, J. Malig, F. Lodermeier, S. Feihl, A. Roth, L. Wibmer, M. Kehrner, M. Volland, P. Wagner, G. G. Wallace, D. L. Officer and D. M. Guldi, *Chem. Sci.*, 2013, **4**, 3085-3098.
3. R. D. Costa, F. Lodermeier, R. Casillas and D. M. Guldi, *Energy Environ. Sci.*, 2014, **7**, 1281-1296.
4. J. Nelson, *Phys. Rev. B*, 1999, **59**, 15374-15380.

5. S. Soedergren, A. Hagfeldt, J. Olsson and S.-E. Lindquist, *J. Phys. Chem.*, 1994, **98**, 5552-5556.
6. T. W. Hamann, R. A. Jensen, A. B. F. Martinson, H. Van Ryswyk and J. T. Hupp, *Energy Environ. Sci.*, 2008, **1**, 66-78.
7. A. M. Spokoyny, T. C. Li, O. K. Farha, C. W. Machan, C. She, C. L. Stern, T. J. Marks, J. T. Hupp and C. A. Mirkin, *Angew. Chem. Int. Ed.*, 2010, **49**, 5339-5343.
8. G. de la Torre, G. Bottari, M. Sekita, A. Hausmann, D. M. Guldi and T. Torres, *Chem. Soc. Rev.*, 2013, **42**, 8049-8105.
9. M. Gong, Y. Li, H. Zhang, B. Zhang, W. Zhou, J. Feng, H. Wang, Y. Liang, Z. Fan, J. Liu and H. Dai, *Energy Environ. Sci.*, 2014, **7**, 2025-2032.
10. J. Cho, N. Salleh, C. Blanco, S. Yang, C.-J. Lee, Y.-W. Kim, J. Kim and J. Liu, *Nanoscale*, 2014, **6**, 3861-3867.
11. R. W. Fessenden and P. V. Kamat, *J. Phys. Chem.*, 1995, **99**, 12902-12906.
12. L. Forro, O. Chauvet, D. Emin, L. Zuppiroli, H. Berger and F. L'vy, *J. Appl. Phys.*, 1994, **75**, 633-635.
13. C. A. Grimes, *J. Mater. Chem.*, 2007, **17**, 1451-1457.
14. L. Kavan, M. Grätzel, S. E. Gilbert, C. Klemenz and H. J. Scheel, *J. Am. Chem. Soc.*, 1996, **118**, 6716-6723.
15. P. Wagner and R. Helbig, *J. Phys. Chem. Solids*, 1974, **35**, 327-335.
16. B. Liu and E. S. Aydil, *J. Am. Chem. Soc.*, 2009, **131**, 3985-3990.
17. K. Zhu, N. R. Neale, A. Miedaner and A. J. Frank, *Nano Lett.*, 2006, **7**, 69-74.
18. A. B. F. Martinson, T. W. Hamann, M. J. Pellin and J. T. Hupp, *Chem. Eur. J.*, 2008, **14**, 4458-4467.
19. S. Calnan and A. N. Tiwari, *Thin Solid Films*, 2010, **518**, 1839-1849.
20. L. M. Peter, *Phys. Chem. Chem. Phys.*, 2007, **9**, 2630-2642.
21. H. Wu, L. Hu, T. Carney, Z. Ruan, D. Kong, Z. Yu, Y. Yao, J. J. Cha, J. Zhu, S. Fan and Y. Cui, *J. Am. Chem. Soc.*, 2010, **133**, 27-29.
22. Z. Yang, S. Gao, T. Li, F.-Q. Liu, Y. Ren and T. Xu, *ACS Appl. Mater. Inter. Interfaces*, 2012, **4**, 4419-4427.
23. F.-Q. Liu, K. Zhu, T. Li and T. Xu, *J. Phys. Chem. C*, 2014, **118**, 9951-9957.
24. F.-Q. Liu, H. Wu, T. Li, L. R. Grabstanowicz, K. Amine and T. Xu, *Nanoscale*, 2013, **5**, 6422-6429.
25. J. Van de Lagemaat, N. G. Park and A. J. Frank, *J. Phys. Chem. B*, 2000, **104**, 2044-2052.
26. K. Schwarzburg and F. Willig, *J. Phys. Chem. B*, 1999, **103**, 5743-5746.
27. J. Bisquert, G. Garcia-Belmonte and F. Fabregat-Santiago, *J. Solid State Electrochem.*, 1999, **3**, 337-347.
28. S. Rühle and T. Dittrich, *J. Phys. Chem. B*, 2005, **109**, 9522-9526.
29. Z. Z. Yang, T. Xu, Y. S. Ito, U. Welp and W. K. Kwoko, *J. Phys. Chem. C*, 2009, **113**, 20521-20526.
30. A. B. F. Martinson, T. W. Hamann, M. J. Pellin and J. T. Hupp, *Chem. Eur. J.*, 2008, **14**, 4458-4467.
31. Z. Z. Yang, T. Xu, S. M. Gao, U. Welp and W. K. Kwok, *J. Phys. Chem. C*, 2010, **114**, 19151-19156.
32. Y. Cheng, H. Zhang, S. Lu, C. V. Varanasi and J. Liu, *Nanoscale*, 2013, **5**, 1067-1073.
33. F.-Q. Liu, W.-H. Li, B.-C. Liu and R.-X. Li, *J. Mater. Chem. A*, 2013, **1**, 8037-8044.
34. Z. Yang, S. Gao, W. Li, V. Vlasko-Vlasov, U. Welp, W.-K. Kwok and T. Xu, *ACS Appl. Mater. Inter. Interfaces*, 2011, **3**, 1101-1108.
35. Z. Yang, T. Xu, S. Gao, U. Welp and W.-K. Kwok, *J. Phys. Chem. C*, 2010, **114**, 19151-19156.
36. J. Qian, P. Liu, Y. Xiao, Y. Jiang, Y. Cao, X. Ai and H. Yang, *Adv. Mater.*, 2009, **21**, 3663-3667.
37. S. Guldin, S. Huttner, M. Kolle, M. E. Welland, P. Muller-Buschbaum, R. H. Friend, U. Steiner and N. Tetreault, *Nano Lett.*, 2010, **10**, 2303-2309.
38. A. Klein, C. Körber, A. Wachau, F. Süberlich, Y. Gassenbauer, S. P. Harvey, D. E. Proffit and T. O. Mason, *Materials*, 2010, **3**, 4892-4914.
39. X. Dou, D. Sabba, N. Mathews, L. H. Wong, Y. M. Lam and S. Mhaisalkar, *Chem. Mater.*, 2011, **23**, 3938-3945.
40. S. Gubbala, V. Chakrapani, V. Kumar and M. K. Sunkara, *Adv. Funct. Mater.*, 2008, **18**, 2411-2418.
41. Y. Zhao and K. Zhu, *J. Phys. Chem. Lett.*, 2013, **4**, 2880-2884.
42. K. Zhu, N. Kopidakis, N. R. Neale, J. van de Lagemaat and A. J. Frank, *J. Phys. Chem. B*, 2006, **110**, 25174-25180.
43. M. G. Helander, Z. B. Wang, J. Qiu and Z. H. Lu, *Appl. Phys. Lett.*, 2008, **93**, 193310.
44. Q. Wang, S. Ito, M. Gratzel, F. Fabregat-Santiago, I. Mora-Sero, J. Bisquert, T. Bessho and H. Imai, *J. Phys. Chem. B*, 2006, **110**, 25210-25221.
45. I. Hwang, C. R. McNeill and N. C. Greenham, *J. Appl. Phys.*, 2009, **106**, 094506.